Ir-Base Refractory Superalloys for Ultra-High Temperatures

Y. YAMABE-MITARAI, Y. RO, T. MARUKO, and H. HARADA

The microstructure and compression strengths of Ir-15 at. pct X (X = Ti, Ta, Nb, Hf, Zr, or V) binary alloys at temperatures between room temperature and 1800 °C were investigated to evaluate the potential of these alloys for ultra-high-temperature use. The fcc and $L1_2$ two-phase structures of these alloys were examined by transmission electron microscopy (TEM) and scanning electron microscopy (SEM). The strengths of the Ir-Ta, -Nb, -Hf, and -Zr alloys were above 800 MPa at temperatures up to 1200 °C and about 200 MPa at 1800 °C. The strengths of these alloys under 1000 °C are equivalent to or higher than those of the commercially used Ni-base superalloys, MAR-M247 and CMSX-10. The Nb concentration dependence of strength was investigated using a series of Ir-Nb alloys with Nb concentrations from 0 to 25 at. pct. It was found that the Ir-base alloys were strengthened by $L1_2$ precipitation hardening. The potential of the Ir-base alloys for ultra-high temperature use is discussed.

I. INTRODUCTION

THE temperature capabilities of Ni-base superalloys have been improved by more than 300 °C over the last 50 years[1] and are approaching 1100 °C, with single crystal superalloys having ideally designed microstructures composed of fcc and $L1_2$ phases.[2] In spite of these efforts, however, it is fair to say that a drastic improvement in the temperature capability of superalloys is becoming more difficult due to the rather low melting temperature of Ni, 1453 °C. Considering the ever-increasing demands for materials with higher temperature capabilities for use in gas turbines with higher efficiency, it is of vital importance to seek new alloys to substitute for Ni-base superalloys.

An approach to develop new alloys with capabilities beyond those of Ni-base superalloys is being made with intermetallics or refractory alloys, for example, NiAl-base alloys strengthened by coherent Ni_2AlTi precipitates,[3] W-base HfC dispersion hardening alloys,[4] and Nb-base alloys precipitation hardened by Nb_3Al.[5] However, problems remain with the poor room-temperature ductilities of intermetallics and the poor oxidation resistance of refractory alloys.

As an alternative, platinum group metals are now being considered. From the point of view the intermetallics, AlRu and RuSc with the B2 structure, IrNb and RuTa with the $L1_0$ structure,[6] and Ir_3Nb and Ir_3Zr[7] with the $L1_2$ structure have been noted. We have proposed a new class of alloys using platinum group metals, which we term ''refractory superalloys.''[8,9] We define this new concept as alloys with fcc and $L1_2$ two-phase coherent structures similar to those in Ni-base superalloys, and yet with considerably higher melting temperatures, since it is well known that $L1_2$ single-phase alloys, as well as fcc single-phase alloys, are less resistant to creep deformation compared with the fcc and $L1_2$ two-phase alloys in Ni-base superalloys.[10] Platinum group metals are ideal as base elements in refractory superalloys due to their melting temperatures (Os: 3045, Ir: 2443, Ru: 2250, Rh: 1960, Pt: 1769, and Pd: 1552 °C, all higher than that of Ni: 1453 °C[11]) and superior oxidation resistance to refractory metals, *i.e.*, Nb, Mo, Ta, and W. Of the platinum group metals, Ir, Rh, Pt, and Pd have the fcc structure, while Os and Ru have the hcp structure. In the Ir-Nb (Figure 1) and Ir-Ti systems, the fcc structure can be equilibrated with the $L1_2$ structure according to binary phase diagrams.[12] The compression strengths of these alloys at 1800 °C were previously investigated.[8] The strengths of these alloys were about 200 MPa at 1800 °C. These data show that Ir-base alloys have a good potential as materials for use at ultra-high temperatures for which Ni-base superalloys are not suitable.

In the present article, an extended investigation was made with other Ir binary systems, where the fcc structure can be equilibrated with the $L1_2$ structure, for example, the Ir-Ta, Ir-Hf, Ir-Zr, and Ir-V systems. The microstructure evolution and mechanical properties at temperatures up to 1800 °C in these alloys were investigated, and the potentials of these alloys for ultra-high temperature use are discussed.

II. EXPERIMENTAL PROCEDURES

Pure Ir and Ir-Nb binary alloys with different Nb contents, from 5 to 25 at. pct, and Ir binary alloys with nominal compositions between 12 and 18 at. pct X (X = Ti, Ta, Hf, Zr, or V) were studied. All the binary alloys were prepared as 150-g button ingots by arc melting in an argon atmosphere.

To understand microstructure at high temperatures, cylindrical samples with 3-mm diameters were cut from the binary alloy ingots and heated at 1200 °C, 1500 °C, and 1800 °C for up to 1 week in an argon atmosphere. The heating at 1200 °C was carried out with these samples encapsulated in quartz tubes filled with argon gas, followed by water quenching. For the heat treatments at 1500 °C and 1800 °C, the entire sequence of heating and cooling was carried out within a vacuum furnace. The microstructures of the samples were observed by scanning electron microscopy (SEM) after electrolytically etching in an ethyl alcohol solution of 5 pct HCl. Thin discs were cut from the heat-treated samples and ion milled for observation by trans-

Y. YAMABE-MITARAI, Researcher, Y. RO, Senior Researcher, and H. HARADA, Group Leader, are with the 3rd Group, National Research Institute for Metals, Ibaraki 305, Japan. T. MARUKO, Engineer, is with the Furuya Metals Co. Ltd., Ibaraki 308, Japan.

Manuscript submitted February 12, 1997.

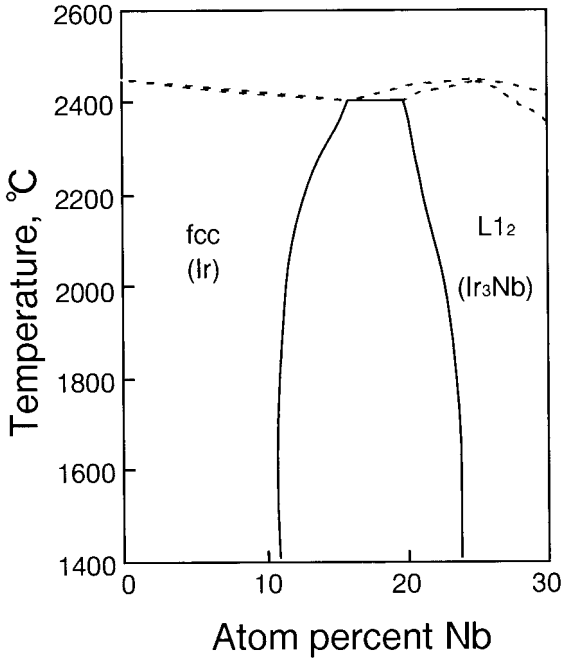

Fig. 1—The phase diagram for the Ir-Nb system.[12]

mission electron microscopy (TEM). All images were taken in the beam direction of [001]. All dark-field images were taken with superlattice reflections (**g** = 110) from the $L1_2$ phase. Some of the Ir alloys were analyzed using an analytical electron microscope with a beam size of 17.5 nm.

Cylindrical samples, 4 mm in diameter and 8 mm in height, were cut from each binary alloy ingot and pure Ir ingot for compression testing. Compression tests were carried out in air for tests at temperatures up to 1200 °C and in an argon atmosphere for tests at 1800 °C. For tests at temperatures higher than room temperature, the samples were kept at the testing temperature for 15 minutes before loading. The initial compressive strain rate for each test was 3.0×10^{-4}/s.

III. RESULTS

A. *Microstructure*

As-cast samples of the Ir-base alloys with second element contents between 15 and 18 at. pct were observed by SEM (Figure 2). A dendritic structure was observed for all except for the Ir-15 at. pct V alloy (not shown). The microstructure of the Ir-15 at. pct V alloy appeared to be a single phase with smooth grain boundaries. Fine precipitates were observed in the dendrite arms in the Ir-15 at. pct Ti alloy (Figure 2(a)). Fine precipitates were observed in the interstices between dendrite arms instead of in dendrite arms in the Ir-18 at. pct Ta alloy (Figure 2(b)). These fine precipitates show that the fcc and $L1_2$ two-phase structures is formed in as-cast samples in the Ir-15 at. pct Ti and Ir-18 at. pct Ta alloys. Precipitates were not observed in the Ir-17 at. pct Nb, Ir-15 at. pct Hf, and Ir-15 at. pct Zr alloys (Figures 2(c) through (e)). A lamellar structure, rather than precipitates, was observed in the interstices between dendrite arms in the Ir-15 at. pct Zr alloy (Figure 2(e)). In contrast, the lamellar structure was not observed in the Ir-15 at. pct Hf alloy.

The secondary electron images of Ir-base alloys, with second element contents of 15 at. pct, heat treated at 1200 °C for 1 week are shown in Figure 3. A dendritic structure within grains with irregular boundaries in the Ir-15 at. pct Ti, -Ta, and -Nb alloys remained after the heat treatment (Figures 3(a) through (c)). In the Ir-15 at. pct Hf and Ir-15 at. pct Zr alloys, precipitates were observed at grain boundaries (Figures 3(d) and (e)). Figure 4 illustrates the microstructures near grain boundaries in the Ir-15 at. pct Hf and Ir-15 at. pct Zr alloys. A lamellar structure was observed on grain boundaries in both alloys. Detailed microstructures within the grains of the Ir-base alloys are shown in Figure 5. Fine precipitates about 100 nm in size were observed in the grains of the Ir-15 at. pct Ti, -Ta, and -Nb alloys (Figures 5(a) through (c)). In contrast, platelike precipitates were observed in the grains of the Ir-15 at. pct Hf and Ir-15 at. pct Zr alloys (Figures 5(d) and (e)). No precipitates were observed in the Ir-15 at. pct V alloys.

The precipitate shapes of the Ir-15 at. pct Ta, -Nb, -Hf, -Zr and -V alloys after heat treatment at 1200 °C for 1 week were studied with TEM (Figure 6). The phases with bright contrast were Ir_3Nb, Ir_3Zr, and Ir_3V with the $L1_2$ structure (Figures 6(b), (d), and (e), respectively). Bright-field images of the Ir-Ta and Ir-Hf alloys were taken (Figures 6(a) and (c)), since it is difficult to detect superlattice reflections from the $L1_2$ structures of these alloys due to the closer atomic scattering factors of Ir, Ta, and Hf resulting in very small structure factors of the superlattices in the $L1_2$ structures. Cubelike precipitates between 100 and 200 nm in size were observed in the Ir-15 at. pct Ta and Ir-15 at. pct Nb alloys (Figures 6(a) and (b)). Cubelike precipitates were surrounded by finer precipitates about 20 nm in size in the Ir-15 at. pct Nb alloy. Since they are also observed in Ni-base superalloys, we conclude that the fine precipitates were formed in the matrix during cooling. Platelike precipitates were formed in the Ir-15 at. pct Hf and Ir-15 at. pct Zr alloys (Figures 6(c) and (d)), although whether it was the bright or the dark contrast phase in the Ir-15 at. pct Hf alloy that had the $L1_2$ structure is not clear. In the Ir-15 at. pct V alloy, irregularly shaped precipitates, 10 nm in size, were observed (Figure 6(e)), although precipitates were not observed by SEM. The habit planes in these Ir-base alloys were close to {100} planes independent of precipitate shape (Figure 6). Cube and platelike precipitates were observed in the Ir-15 at. pct Nb and -Zr alloys, respectively, after heat treatment at 1200 °C for 1 hour. We conclude that the $L1_2$ precipitates formed during heating before compression testing in the Ir-Nb and -Zr, and also other alloys, although precipitates, were not observed in the as-cast samples.

The concentration of Ta in the Ir-15 at. pct Ta alloy was examined by analytical TEM to determine whether the $L1_2$ structure exists, since it is difficult to detect $L1_2$ superlattice reflections in this alloy. Relatively large precipitates were selected for analysis. The concentration of Ta in the matrices were 15.4 and 15.2 at. pct and those of the precipitates were 23.3, 23.0, 23.2, 23.1, and 23.4 at. pct, although the absolute composition is not clear since a standard specimen was not used. For a concentration of 23 at. pct Ta, Ir_3Ta is the equilibrium phase predicted from the phase diagram, suggesting that the precipitates were Ir_3Ta. The fine microstructure of the Ir-Hf alloy made analysis of either phase difficult.

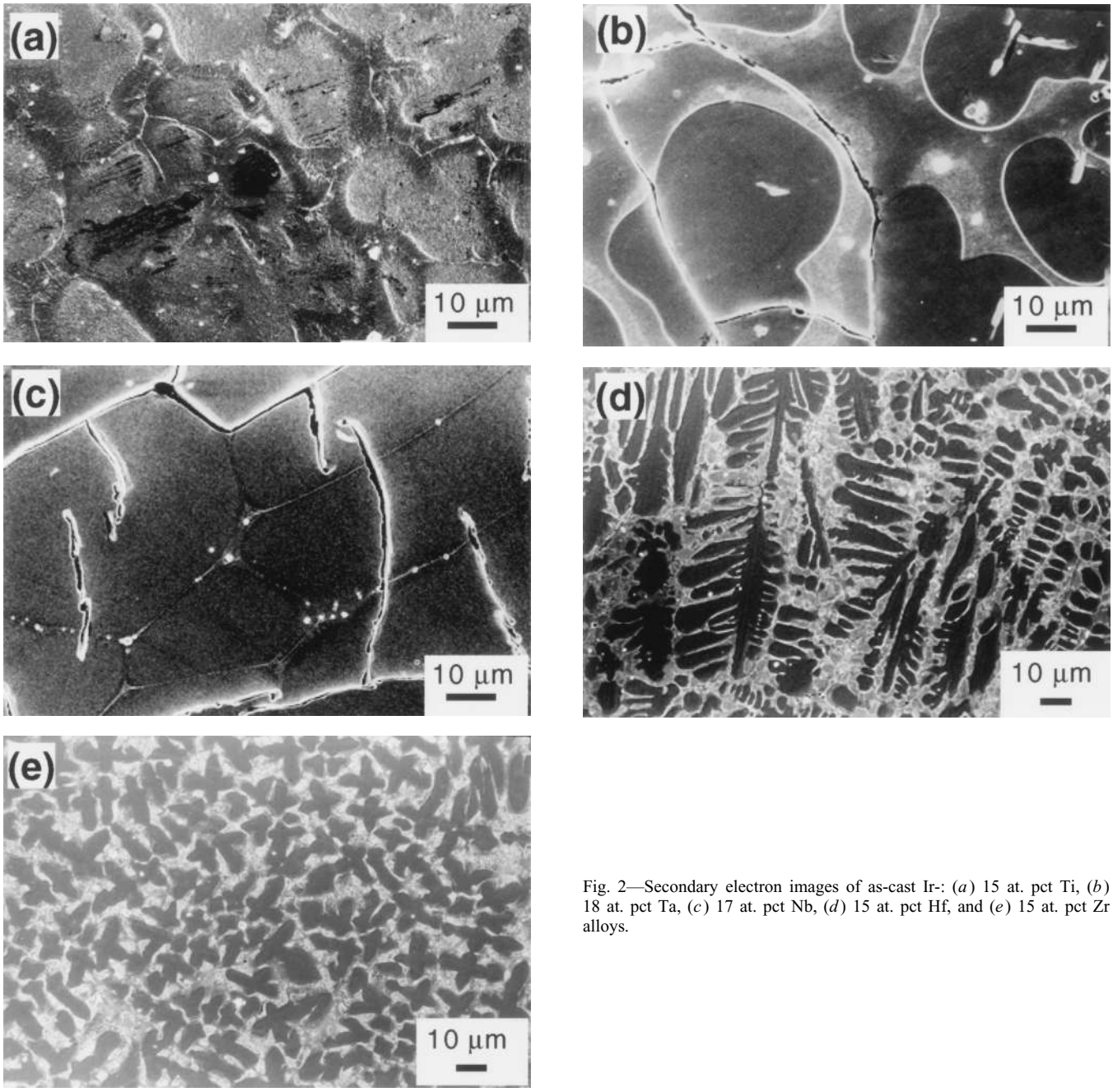

Fig. 2—Secondary electron images of as-cast Ir-: (*a*) 15 at. pct Ti, (*b*) 18 at. pct Ta, (*c*) 17 at. pct Nb, (*d*) 15 at. pct Hf, and (*e*) 15 at. pct Zr alloys.

Despite clear detection of $L1_2$ superlattice reflections in TEM images of the Ir-Ti alloy, it was difficult to clearly observe the shape of the precipitates. Previously,[8] we investigated the crystal structure of the Ir-15 at. pct Ti alloy heated at 1800 °C for 3 hours using X-ray powder diffractometry and found that it also has the fcc and $L1_2$ two-phase structures.

B. *Compression Test*

The as-cast Ir-15 at. pct X alloys (X = Ti, Ta, Nb, Hf, Zr, or V) were compressed at room temperature, 1200 °C, and 1800 °C until samples failed or reached 15 pct strain (Figure 7). At room temperature, the alloys were classified into three distinct groups on the stress-strain curve (Figure 7(a)). The alloys of the first group, the Ir-15 at. pct Nb and Ir-15 at. pct Hf, were strong (above 800 MPa) and ductile in compression. The second group alloys, Ir-15 at. pct Ta and Ir-15 at. pct Zr, were as strong as those of the first group but brittle. The third group alloys, Ir-15 at. pct Ti and Ir-15 at. pct V, were weak compared with the others, but they were ductile in compression. At 1200 °C, the alloys were still classified into 3 groups, however, in different combinations (Figure 7(b)). The Ir-15 at. pct Ti and Ir-15 at. pct V alloys were ductile and weak, just as at room temperature. The Ir-15 at. pct Hf and Ir-15 at. pct Zr alloys were ductile despite their strength, although the samples failed after about 5 and 15 pct strain, respectively. The Ir-15 at. pct Nb and Ir-15 at. pct Ta alloys were strong but suffered brittle failure under 1000 MPa. At 1800 °C, the Ir-

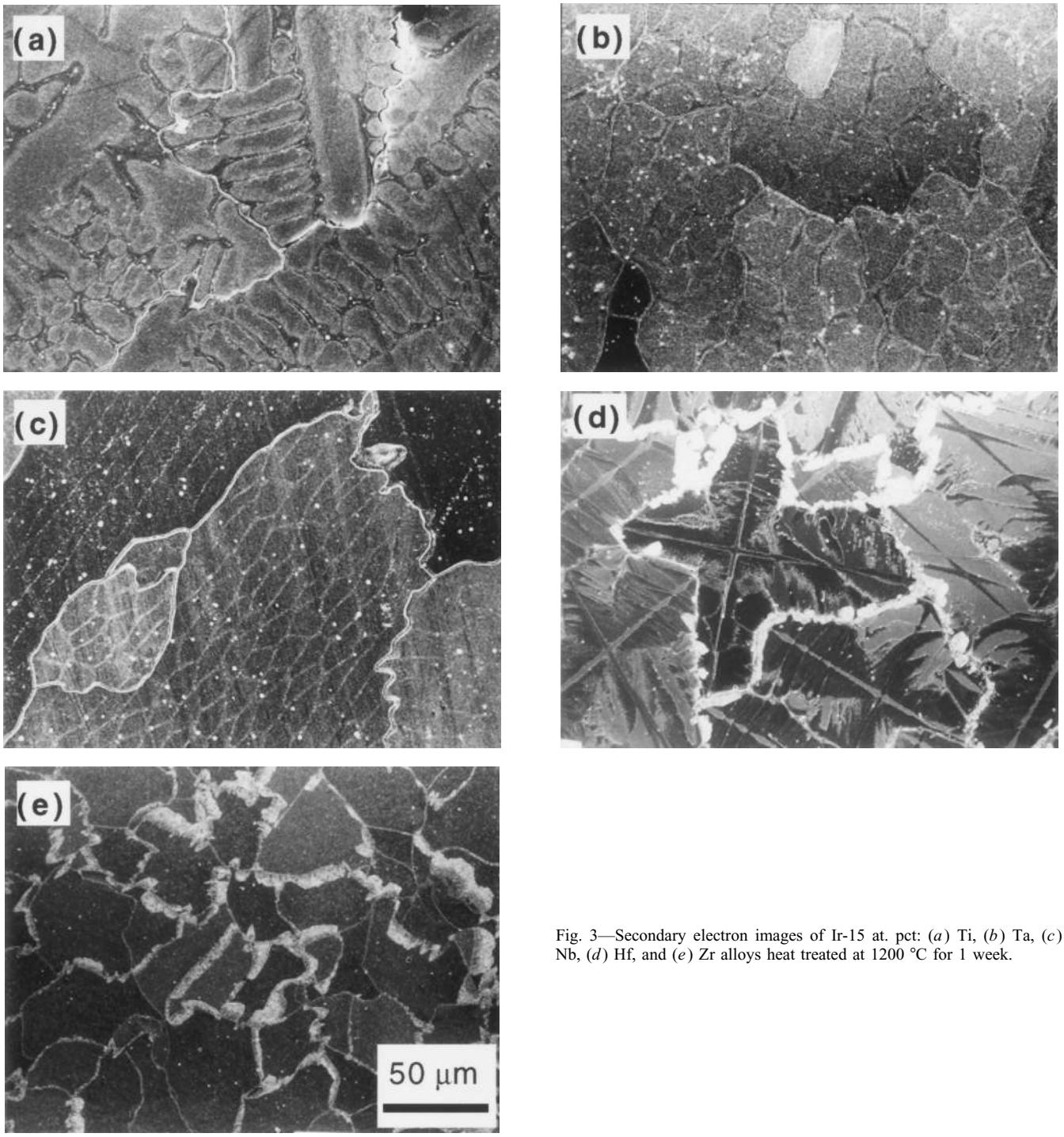

Fig. 3—Secondary electron images of Ir-15 at. pct: (*a*) Ti, (*b*) Ta, (*c*) Nb, (*d*) Hf, and (*e*) Zr alloys heat treated at 1200 °C for 1 week.

15 at. pct V alloy was weak and ductile (Figure 7(c)). The Ir-Hf alloy remained strong and ductile in compression at this temperature. The shapes of the curves for the other four alloys were similar to each other, they were strong but failed after a few percent strain.

Temperature dependence of the 0.2 pct flow stress in as-cast Ir-15 at. pct X alloys (X = Ti, Ta, Nb, Hf, Zr, or V) is shown in Figure 8. The 0.2 pct flow stresses of a Ni-Al-Cr alloy with 40 pct $L1_2$ phase[13] (a base for development of Ni-base superalloys), a commercially available Ni-base superalloy, and MAR-M247 (Ni-10Co-10W-8.5Cr-5.5Al-0.7Mo-3Ta-1.4Hf, wt pct)[4] and the tensile yield stresses of a third generation single-crystal Ni-base superalloy, CMSX-10 (Ni-2Cr-3Co-0.4Mo-5W-8Ta-6Re-0.1Nb-5.7Al-0.2Ti-0.03Hf wt pct),[14] and of a W-base HfC dispersion hardening alloy (W-0.35 wt pct Hf-0.025 wt pct C)[4] are also shown for reference (Figure 8). The strengths of Ni-base superalloys decreased drastically with increasing temperature above 800 °C. Although the strengths of the Ir-15 at. pct Nb, -Ta, -Hf, and -Zr alloys

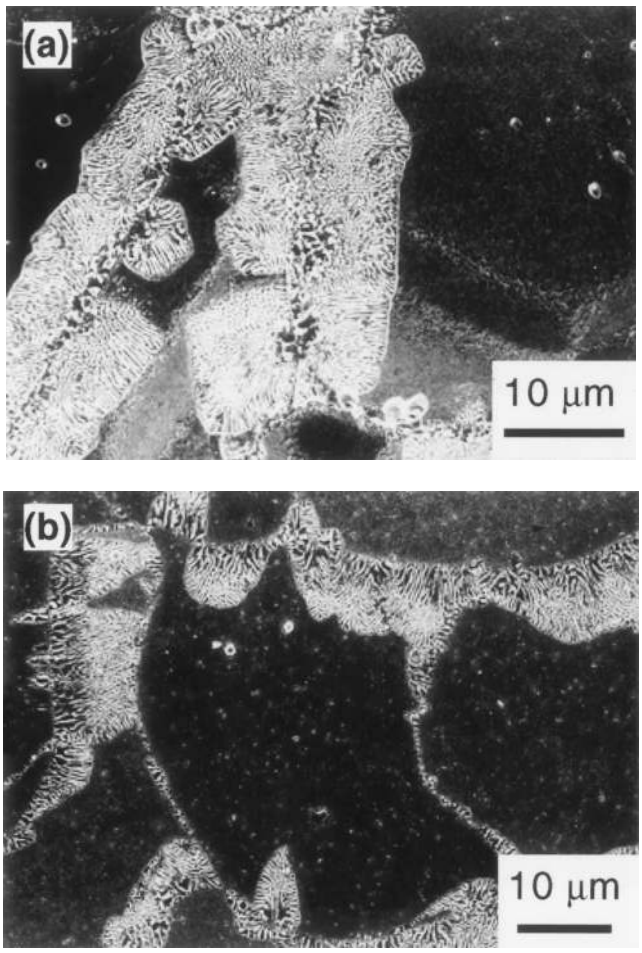

Fig. 4—Secondary electron images of Ir-15 at. pct: (*a*) Hf and (*b*) Zr alloys heat treated at 1200 °C for 1 week.

also decreased with increasing testing temperature, at room temperature and 1200 °C, they were equivalent to or far higher than the strengths of MAR-M247* and CMSX-10.

*MAR-M247 is a trademark of Lockheed Martin, Baltimore, MD.

The 0.2 pct flow stress of these four Ir-base alloys was above 800 MPa even at 1200 °C, much higher than that of MAR-M247 (50 MPa) at that temperature. At 1800 °C, the strength of the four Ir-base alloys was about 200 MPa, equivalent to the strength of the W-HfC alloy (197 MPa), which had been the strongest metallic material available at this temperature. The strengths of the Ir-15 at. pct Ti and Ir-15 at. pct V alloys were low at all tested temperatures. Note that among the Ir alloys tested here, only the Ir-15 at. pct V alloy has an fcc single phase at 1800 °C according to the phase diagram.[12]

The series of the as-cast Ir-Nb alloys with the Nb concentration from 0 to 25 at. pct were also compressed at room temperature, 1200 °C, and 1800 °C. At 1800 °C, the stress-strain curve of swaged pure Ir is shown by the dotted line for references since we do not have any data of as-cast pure Ir at 1800 °C. The 0.2 pct flow stress of all Ir-Nb alloys was higher than that of pure Ir at any temperature (Figure 9). At all tested temperatures, the strength of the Ir-15 at. pct Nb alloy, which has the fcc and $L1_2$ two-phase structures, was higher than those of the Ir-10 at. pct Nb alloy with the fcc single-phase structure and the Ir-25 at. pct Nb alloy with the $L1_2$ single-phase structure. All the Ir-Nb alloys had compression strains above 10 pct at room temperature, although the samples failed during the test. Ductility improved at 1800 °C in the Ir-25 at. pct Nb alloy with the $L1_2$ single-phase structure.

We evaluated the temperature dependence of 0.2 pct flow stress from stress-strain curves in Ir-Nb alloys with Nb contents between 0 and 25 at. pct (Figure 10). Strength decreased with increasing temperature for all Ir-Nb alloys. The strengths of the alloys with Nb contents above 10 at. pct were similar to those of the Ni-base superalloys shown in Figure 8.

IV. DISCUSSION

A. *Microstructure*

The most important aspect of the microstructure in the Ir-base alloys is the coherency of the interface between the fcc and $L1_2$ phases. If the interface is semicoherent, misfit dislocations can be observed on the interface. No dislocations were observed in any of the Ir-base alloys we studied. Our observations indicate that the interface is either perfectly coherent or incoherent. We conclude that the interface is coherent, since the precipitates were surrounded by {100} planes, like Ni-base superalloys in which the cubic precipitates are formed with coherent interfaces, {100}. When the precipitates are incoherent with the matrix, the lattice misfit has no significance. In this case, the shape of the precipitates depends on volume misfit, since elastic strain energy is proportional to the square of the volume misfit.[15] Therefore, the equilibrium shape of incoherent precipitates will be an oblate spheroid, which balances interfacial energy and strain energy.

The shape of the precipitates depends on the lattice misfit between the precipitates and matrix in the Ir-base alloys. The lattice misfit of the Ir-V, -Ti, -Ta, -Nb, -Hf, and -Zr alloys calculated using the lattice parameters of Ir and Ir_3X (X = V, Ti, Ta, Nb, Hf, and Zr), 0.3839, 0.3812, 0.3843, 0.3884, 0.3892, 0.3933, and 0.3941 nm, respectively,[16] are −0.7, 0.1, 1.04, 1.4, 2.4, and 2.7 pct, respectively. The Ir-Hf and Ir-Zr alloys with large lattice misfits have platelike precipitates. In Ni-base superalloys, cubic precipitates are often observed since the lattice misfit is less than 1 pct. Thompson *et al.* showed by calculation that the interfacial energy and elastic energy are related to lattice misfits between the matrix and the precipitates and that the shapes of precipitates change from fourfold symmetric to twofold symmetric in two dimensions to reduce total energy when the precipitates grow large.[17] Thus, it seems reasonable to expect that when the precipitates have a large lattice misfit with the matrix, the precipitate shapes become platelike to reduce the strain energy of the interface. The reason the precipitate shape of the Ir-V alloy was irregular is probably due to the small lattice misfit.

In the Ir-Hf and Ir-Zr alloys with large lattice misfits, not only platelike precipitates but also lamellar structures at grain boundaries were observed after a aging for a long time. We conclude the lamellar structures were formed by discontinuous coarsening. In the Ir-15 at. pct Zr alloy, a

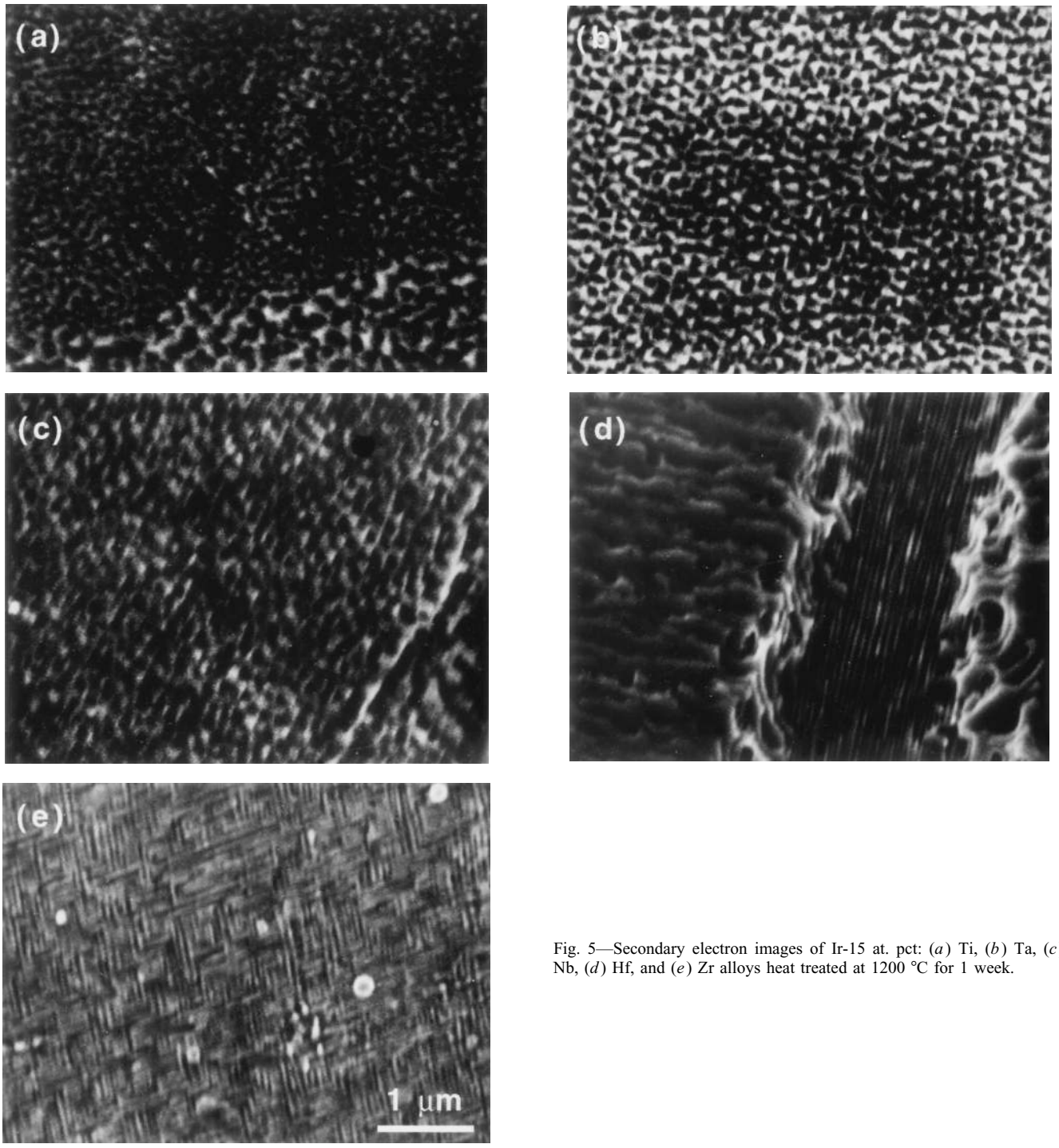

Fig. 5—Secondary electron images of Ir-15 at. pct: (*a*) Ti, (*b*) Ta, (*c*) Nb, (*d*) Hf, and (*e*) Zr alloys heat treated at 1200 °C for 1 week.

lamellar structure was observed clearly even in the as-cast sample. However this lamellar structure disappeared in the sample heat treated at 1200 °C for 1 hour and was observed again in the sample heat treated for over 10 hours with a volume fraction of about 10 pct. This observation shows that the lamellar structure at grain boundaries in heat-treated samples was formed by discontinuous coarsening during heat treatment. It is known that discontinuous coarsening occurs in the Ni-base superalloys with large lattice misfits.[2] When the lattice misfit on the coherent interface between the fcc and $L1_2$ phases is large, the strain energy on the interface becomes very high. Thus, the precipitates coarsen discontinuously in order to reduce strain energy in Ni-base superalloys with large lattice misfits. In the Ir-base alloys, the lamellar structure at grain boundaries was observed only in the Ir-15 at. pct Hf and Ir-15 at. pct Zr alloys with large lattice misfits. We attribute the formation of the lamellar structures to discontinuous coarsening, as occurs in Ni-base superalloys.

The microstructure of the Ir-15 at. pct Hf alloy is very complex; in addition to the lamellar structure caused by discontinuous coarsening, the grain shape is not spherical

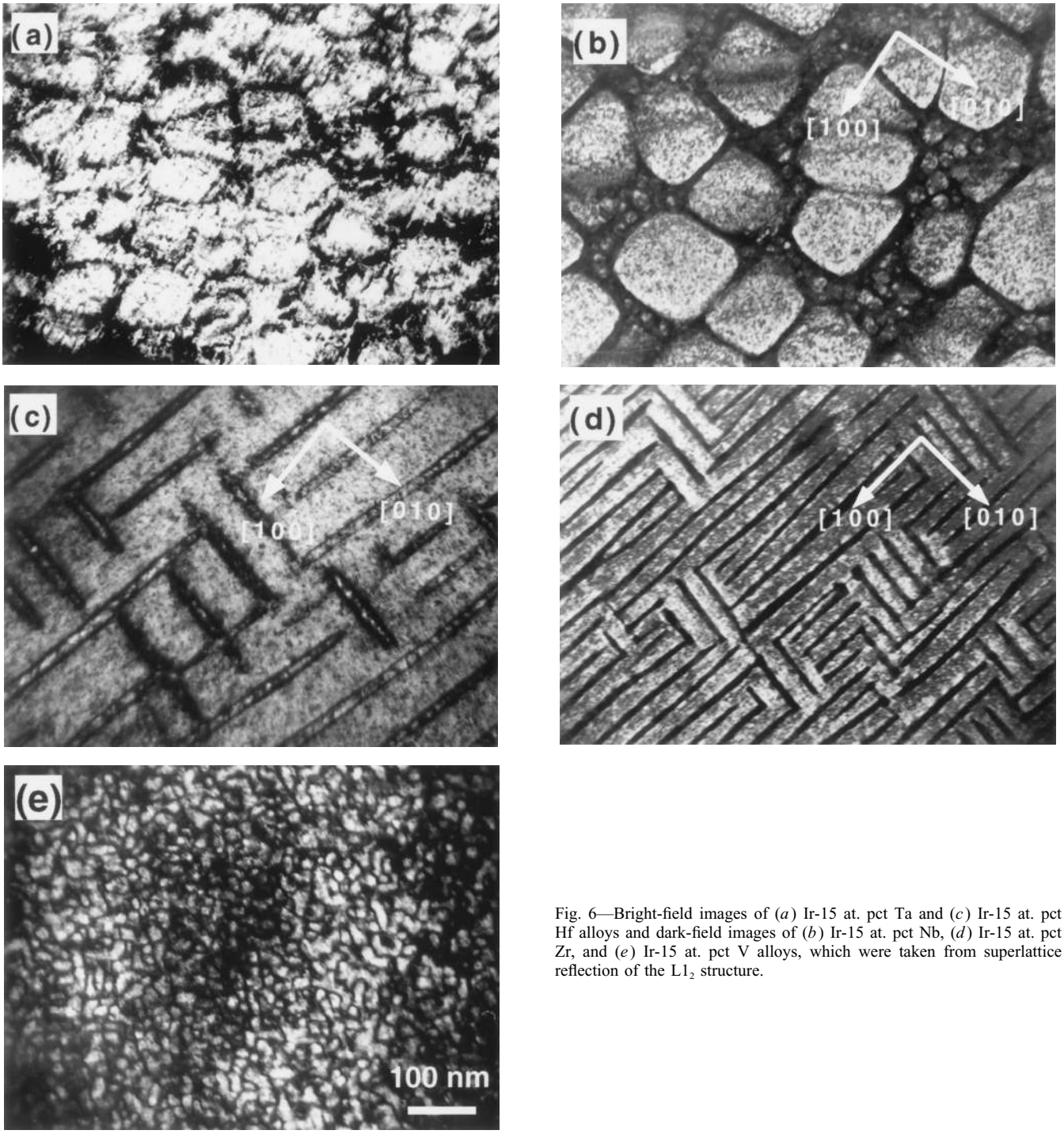

Fig. 6—Bright-field images of (*a*) Ir-15 at. pct Ta and (*c*) Ir-15 at. pct Hf alloys and dark-field images of (*b*) Ir-15 at. pct Nb, (*d*) Ir-15 at. pct Zr, and (*e*) Ir-15 at. pct V alloys, which were taken from superlattice reflection of the $L1_2$ structure.

but rather the cross section of a dendrite (Figure 3(d)). Samples of the Ir-15 at. pct Hf alloy heat treated at 1500 °C for 1 week and at 1800 °C for 1 hour were examined to understand microstructure evolution (Figure 11). After the 1500 °C heat treatment, some contrast inside the grains remained. However, the grain shape became more spherical than that in the case of heat treatment at 1200 °C because diffusion is faster at 1500 °C. After heat treatment at 1800 °C for 1 hour, the dendritic structure remained like that found in as-cast samples, because the heat treatment time was too short for this structure to be lost. This observation shows that as-cast dendrites still remained in the heated samples. The structure inside the grains may be caused by a concentration gradient within the dendrites.

B. *Strength Behavior in Ir-Base Alloys*

We investigated the dependence of Nb concentration on the strength in Ir-Nb alloys (Figure 12). Up to 10 at. pct Nb, the alloys have the fcc single phase. The $L1_2$ single phase exists in the Ir-25 at. pct Nb alloy. The fcc and $L1_2$ two-phase regions exist in alloys with concentrations be-

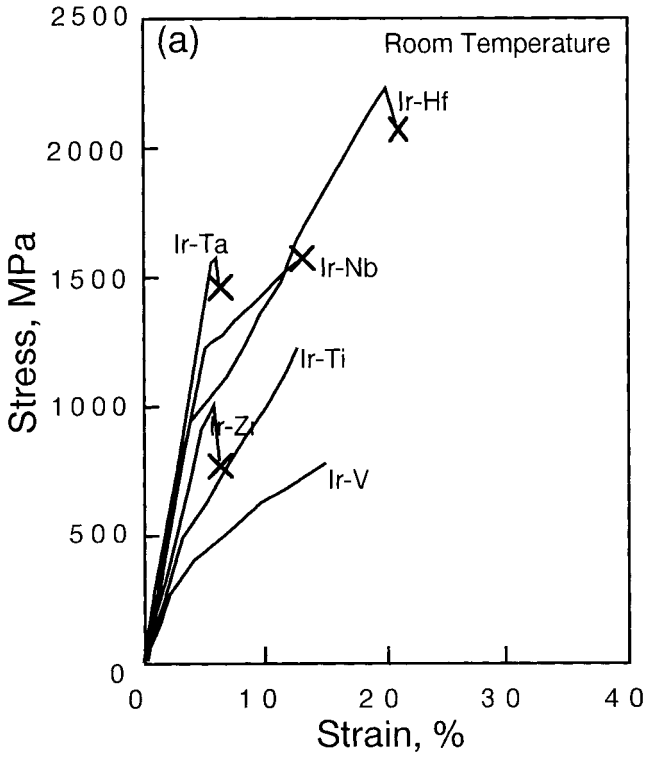

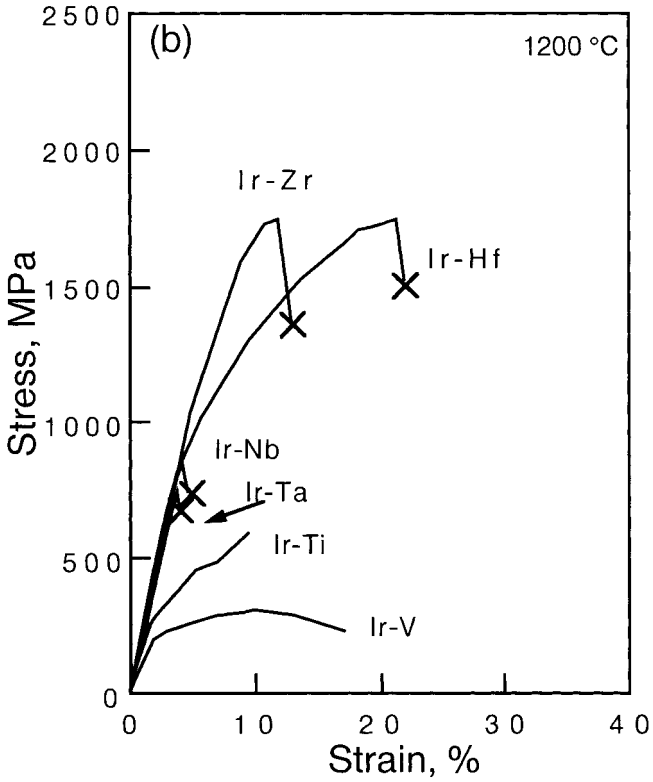

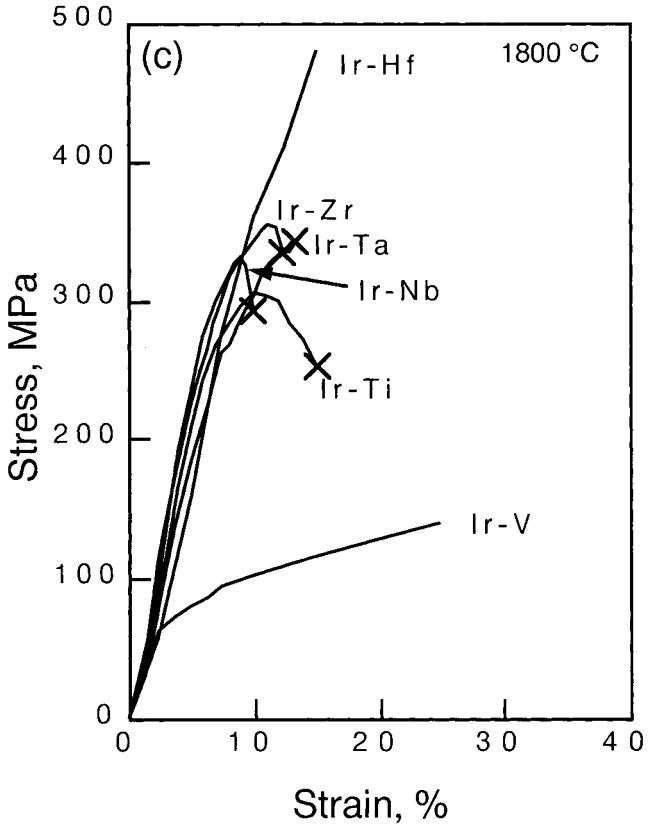

Fig. 7—The compressive stress-strain curves of as-cast Ir-15 at. pct X alloys (X = Ti, Ta, Nb, Hf, Zr, or V) at (*a*) room temperature, (*b*) 1200 °C, and (*c*) 1800 °C. Cross symbol shows that the sample was failed during the test.

tween 10 and 23 at. pct Nb. In the fcc single phase, strength increased gradually with increasing Nb concentration, suggesting that Nb acts not only as an $L1_2$ precipitate former element, but also as a solid solution hardener in Ir. We attribute the further strengthening achieved by adding Nb to 15 at. pct to the precipitation hardening of the $L1_2$ phase or to the fcc and $L1_2$ coherent two-phase interface preventing dislocation movement, as occurs in Ni-base superalloys.[10,18] In the Ir-Nb alloys, we can estimate the solid solution hardening effect in the two-phase alloys. The fcc matrix and $L1_2$ precipitates in two-phase alloys should be in equilibrium with each other, the chemical compositions

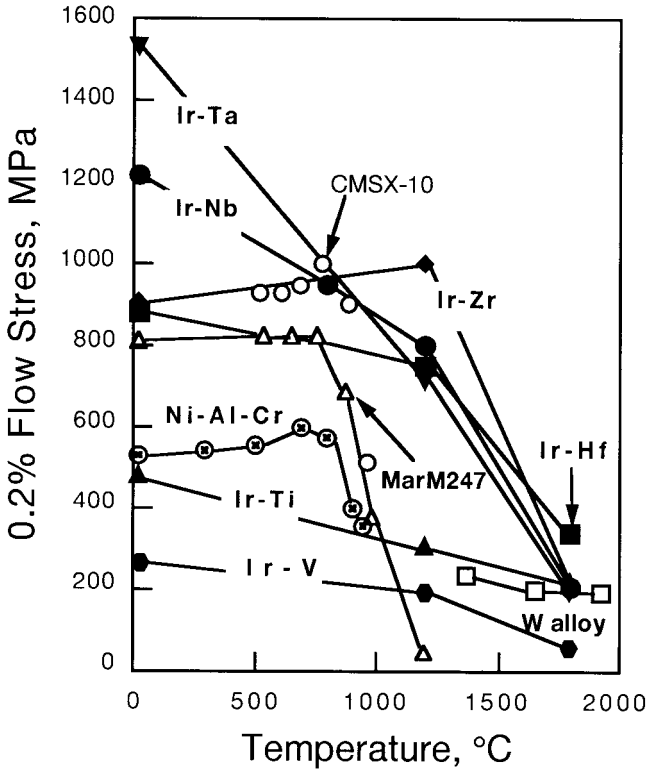

Fig. 8—Temperature dependence of 0.2 pct flow stress during compression testing in as-cast Ir-15 at. pct X alloys (X = Ti, Ta, Nb, Hf, Zr, or V) and Ni- and W-base alloys.

of the phases being about 10 and 23 at. pct Nb, respectively. The contribution by solid solution hardening can be estimated by the law of mixture in strength of composite materials, as a linear combination of the strengths of the fcc matrix and the $L1_2$ precipitates. The peak strength of the two-phase alloys is higher than the strength thus estimated by the law of mixture. The difference between the experimentally determined strength and the strength by solid solution hardening is due to precipitation hardening.

It is well known that the creep strength of single-crystal Ni-base superalloys depends on lattice misfit between the fcc and $L1_2$ precipitates. The negative lattice misfit was effective in improving the creep rupture life[19,20] in single-crystal Ni-base superalloys. For example, the experimental Ni-base superalloy TMS-63 with negative lattice misfit of around −0.25 pct has a longer creep rupture life, 2657 hours under 137 MPa at 1040 °C, than does CMSX-4 (800 hours at 0 pct lattice misfit) and TMS-19 (447 hours, at positive lattice misfit around 0.1 pct). This is because the cuboidal precipitates form plates normal to the [001] stress axis, so-called rafted structure, if tensile stress is applied along the [001] axis of the single-crystal Ni-base superalloys. The rafted structure is effective in improving the creep performance at high temperatures and low stresses when dislocations climb over the precipitates, since the rafted structure increases the length of the climb path.[21] Not only creep strength but also tensile strength depends on precipitate morphology.[22] Tien and Gamble showed that the sample with plate γ' with the $L1_2$ structure perpendicular to the tensile axis [001] is strongest compared with the alloys with γ' cuboid or rod for the tensile test at 6.5×10^{-4}/s using a single crystal of a Ni-base superalloy, UDIMET*-700.

*UDIMET is a trademark of Special Metals Corporation, New Hartford, NY.

Their explanation of the precipitate shape dependence of the strength is given subsequently. The slip system of <100> orientated Ni-base superalloys is normally $\{111\}\langle 1\bar{1}0\rangle$. The interactions between dislocations and particles during deformation can be essentially treated as dislocations interacting with an isolated particle in such high γ' volume fraction alloys as UDIMET-700. Dislocations will try to wrap around each particle and thus result in a force helping to push the dislocation into the particle when dislocations encounter particles. This force reduces the magnitude of the critical resolved shear stress required for dislocation motion. Thus, the force is written as follows:

$$\Delta\tau_s = -\frac{G\mathbf{b}}{2r}$$

where $\Delta\tau_s$ is a term in the CRSS expression, G is the elastic modulus, $\mathbf{b}$ is Burger's vector of dislocation, and r is the radius of spherical particles. The effective radius of curvature on the {111} slip planes of plate γ' approaches infinity. The value of $\Delta\tau_s$ will tend to zero in the preceding equation, since the dislocations coming in contact with these γ' plates will tend to remain straight. Thus, the crystal with plate γ' is the strongest.

The Ir-base alloys include different volume fractions of the $L1_2$ precipitate in our results. Thus, the relationship between lattice misfit and strength in the Ir-base alloys is neither clear nor simple. To clarify the effect of lattice misfit on the strength in Ir-base alloys, the 0.2 pct flow stresses of the Ir-17 at. pct Ti, Ir-18 at. pct Ta, Ir-17 at. pct Nb, and Ir-12 at. pct Zr alloys with 50 pct precipitates in volume fraction were investigated by compression testing at 1200 °C (Figure 13) as a function of lattice misfit. The strength of these Ir-base alloys increased with increasing lattice misfit. A three-dimensional maze structure was formed in the Ir-Zr alloys with large lattice misfit. The three-dimensional maze structure is expected to act as does the rafted structure or plate precipitates, since the effective radius of curvature on the {111} slip planes of the three-dimensional maze structure is expected to be large. Thus, the three-dimensional maze structure is effective in improving tensile or compression strength. Note that unlike the case with Ni-base superalloys, the three-dimensional maze structure is formed in the Ir-Zr and Ir-Hf alloys by simple heat treatment without any thermomechanical processing because of their large lattices. Ro *et al.* showed that the γ' single-phase alloy with the $L1_2$ structure, as well as the γ single-phase alloy with the fcc structure, is less resistant to creep deformation and has lower tensile strength compared with the γ/γ' two-phase alloys using a series of alloys on a γ-γ' tie-line of INCONEL* 713C.[10] We expect that three-dimensional maze structures are effective in preventing motion of dislocation during creep testing in Ir-base alloys, although we need to investigate this further.

*INCONEL is a trademark of INCO Alloys International, Inc., Huntington, WV.

Not only lattice misfit and volume fraction of precipitates

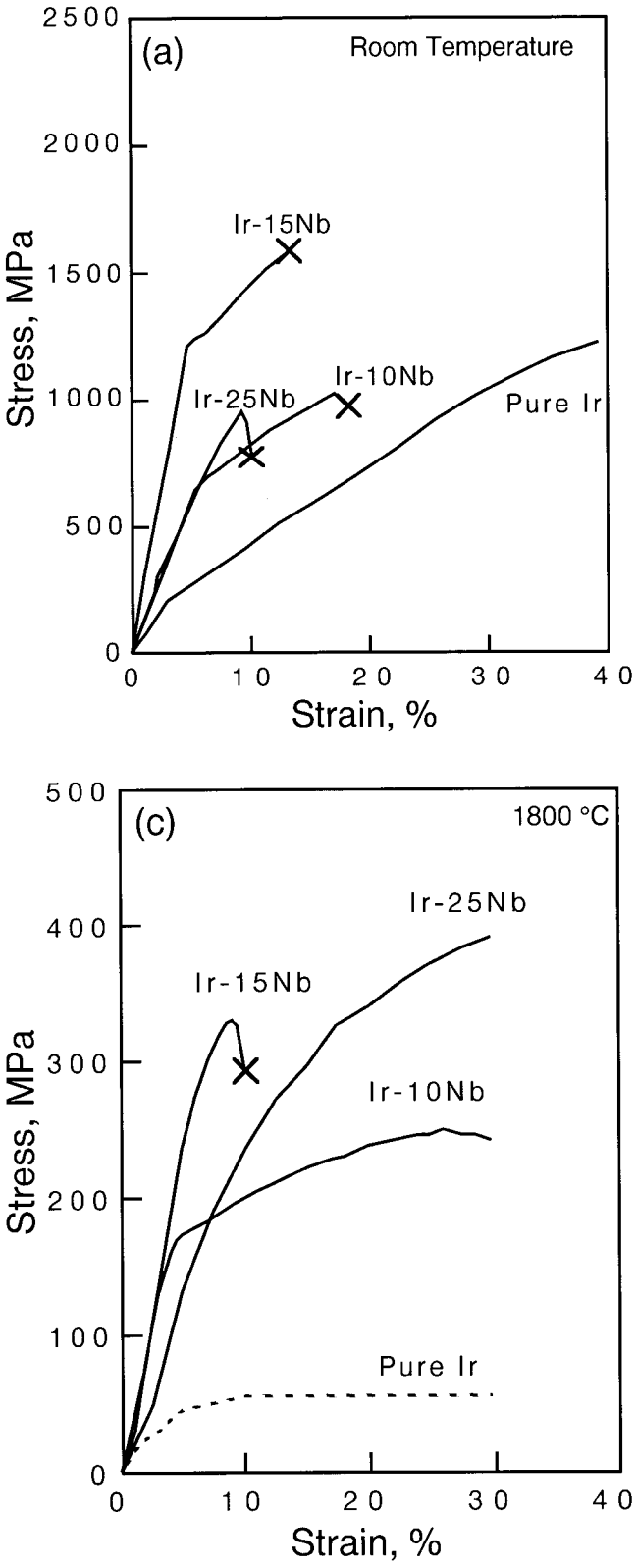

Fig. 9—The stress-strain curve of the Ir-Nb alloys at (*a*) room temperature, (*b*) 1200 °C, and (*c*) 1800 °C. Cross symbol shows that the sample was failed during the test.

but also solid solution hardening and precipitation hardening affect the strength of Ir-base alloys, as shown in the Ir-Nb alloy. The solubility of the second elements to the fcc matrix depends on the alloy system. For example, the solubility limits of binary alloying elements in the Ir-V, -Ti, -Ta, and -Nb alloys are over 10 at. pct at 1400 °C, while only a few atomic percent of Hf and Zr can be dissolved in Ir. This shows that the solid solution hardening effect depends on each system. Differences of the strengths of the $L1_2$ precipitates themselves should also affect the strengths of the alloys with the fcc and $L1_2$ two-phase structures. The fineness of the microstructure, for example, precipitate size,

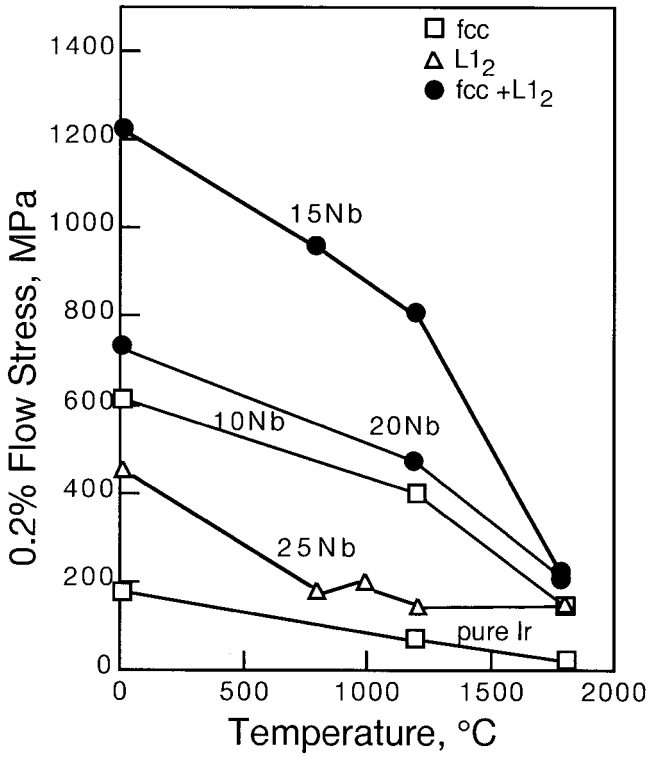

Fig. 10—Temperature dependence of 0.2 pct flow stress during compression testing of as-cast Ir-Nb alloys.

also affects alloy strength. It is necessary to investigate these effects to understand the mechanical properties of Ir-base alloys.

C. *Strength Behavior of Ir_3Nb with $L1_2$ Structure*

The anomalous temperature dependence of strength has been observed in other $L1_2$ structures in Ni_3Si and Co_3Ti,[23] in Ni_3Ga,[24] in Zr_3Al,[25] *etc.*, since Guard and Westbrook first noted the anomalous increase of hardness of Ni_3Al with increasing temperature.[26] In platinum alloys such as Pt_3Sn, Pt_3Ga, Pt_3In, and Pt_3Al, weak anomalous temperature dependence occurs at around 500 °C, with drastic decreases in strength with increasing temperatures below room temperature.[27] For Ir alloys, Bruemmer *et al.*[28] showed that the high-temperature hardness of sputtered thin film Ir_3Nb with 10-nm grains increases with increasing temperature, and the temperature of peak hardness is 800 °C. However, Gyurko and Sanchez[7] showed that hardness and 0.2 pct yield stress during compression testing of Ir_3Nb and Ir_3Zr decrease with increasing temperature. They concluded that Ir_3Nb, with higher ordering energy compared with that of Ni_3Al, should exhibit normal yield behavior since such behavior is expected in systems with high ordering energy. In our results, weak anomalous temperature dependence of the 0.2 pct flow stress in Ir_3Nb with the $L1_2$ structure was observed between 800 °C and 1000 °C (Figure 10). Wee *et al.*[27] suggested that the temperature dependence of strength, positive or negative, is not controlled by antiphase boundary energy itself; antiphase boundary energy correlated strongly with ordering energies. The strength behavior depends on the anisotropy, rather than the magnitude of the antiphase boundary energy. For example, Ni_3Ge, with high antiphase boundary energy, exhibits anomalous temperature dependence. Thus, it is possible to have anomalous temperature dependence of strength for the Ir_3Nb, although further investigation is necessary to detect this behavior clearly. The differences between Gyurko's results and our results are that samples were hot isostatically pressed in Gyurko's results, while our samples were cut from as-cast ingots without hot isostatic pressing. Thus, the grain size of Gyurko's samples is about 10 μm, while the grain size of our samples is over 300 μm. The strengths of our Ir_3Nb samples with 700-μm grain size are lower than those of Gyurko's samples at any testing temperature. They investigated the temperature dependence of the strength by high-temperature microhardness and did not observe anomalous temperature dependence of the strength, while Bruemmer observed anomalous temperature dependence of the strength using thin film Ir_3Nb with 10-nm grains by high-temperature hot hardness. Whether Ir_3Nb shows anomalous temperature dependence of the strength depends on sample preparation or the testing condition. Further investigation is necessary.

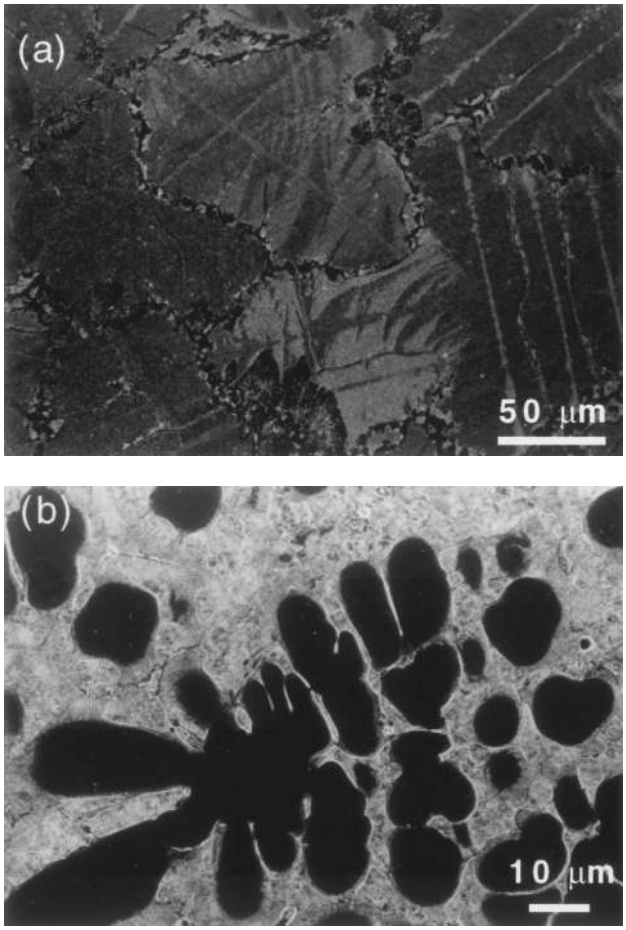

Fig. 11—Secondary electron images of the Ir-15 at. pct Hf alloys heat treated at (*a*) 1500 °C for 1 week and (*b*) 1800 °C for 1 h.

D. *Possibility for High-Temperature Materials*

In addition to mechanical properties and oxidation resistance, physical properties such as thermal expansion, ther-

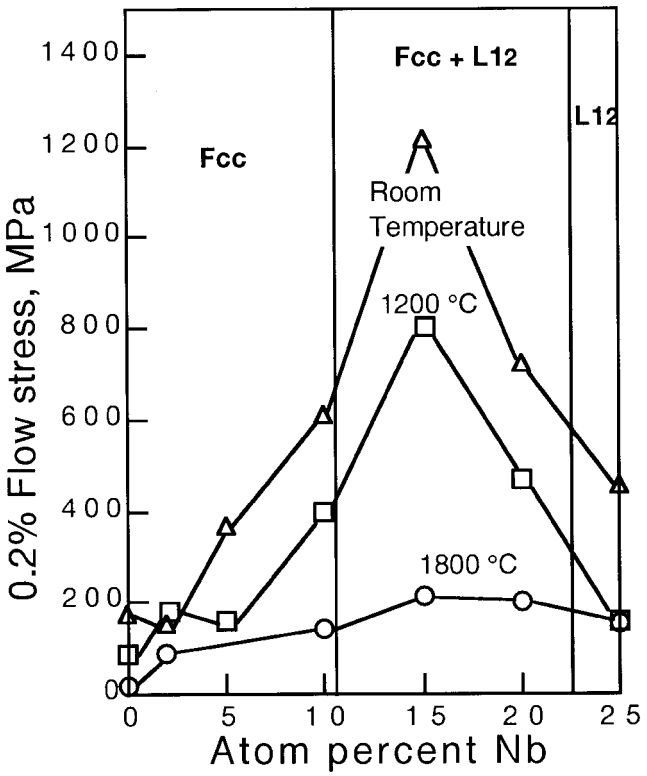

Fig. 12—Nb concentration dependence of 0.2 pct flow stress in as-cast Ir-Nb alloys.

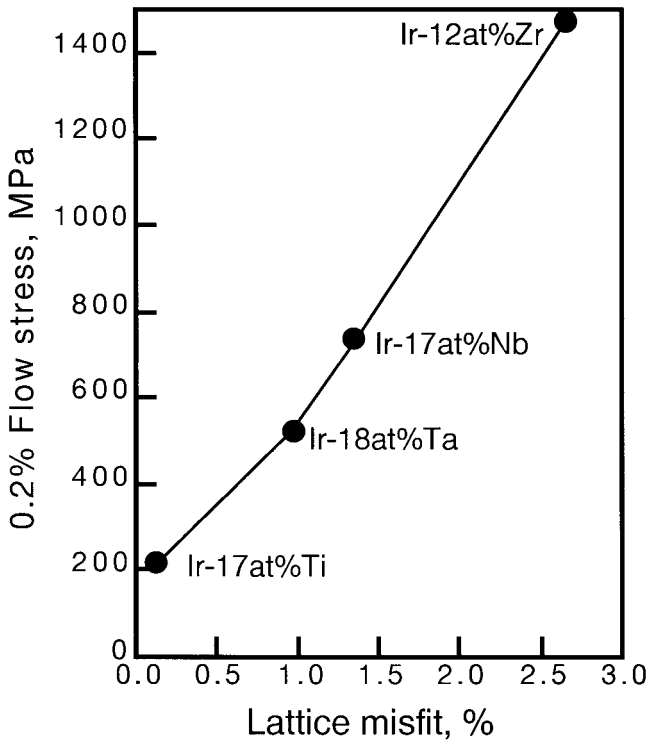

Fig. 13—Lattice misfit dependence of 0.2 pct flow stress during compression testing in as-cast Ir-base alloys with 50 pct $L1_2$ precipitates in volume fraction.

mal conductivity, and elastic modulus are very important when considering new materials for possible use as turbine blades or vanes.[1] Materials with lower thermal expansion, higher thermal conductivity, and lower elastic modulus exhibit superior thermal fatigue resistance. High thermal conductivity also improves cooling efficiency in parts that need internal cooling, such as hollow blades and vanes made of Ni-base superalloys. The physical properties of pure Ni, pure Ir,[29,30] and the superalloy MAR-M200[31] are shown in Table I. Pure Ir has the lowest thermal expansion and highest heat conductivity among these three materials. Iridium with its higher elastic modulus is inferior to Ni with its lower elastic modulus as regards stiffness.

Overall, the Ir-base alloys are promising materials for ultra-high-temperature use. Indeed, the Ir-0.3 pct W alloy has been tried as the primary containment for space power systems or for general purpose heat sources, although this alloy has the fcc single-phase structure.[32] Our Ir-base refractory superalloys are stronger than the Ir-0.3 pct W alloy because of their fcc and $L1_2$ two-phase coherent structures. It should be noted that the Ir-Hf alloy, for example, is not only strong but also ductile in compression at all tested temperatures; it showed nearly 20 pct compression ductility even at room temperature. Furthermore, our results demonstrate that the balance of strength and compressive ductility can be controlled by adjusting the content of the alloying element, for example, the Nb in the Ir-base alloys, although we must investigate the tensile ductility of the Ir-base alloys.

However, we must note some disadvantage to use the Ir-base alloys for high-temperature materials. It may be difficult to use the Ir-base alloys for rotating parts such as turbine blades, where specific strength is important, since the density of the Ir is higher (22.4 g/cm^3) than that of Ni (8.9 g/cm^3). The Ir-base alloys will be more suitable for stator parts such as turbine vanes. The very limited Ir supply in the world (3.6 t per year) makes it difficult to use the Ir-base alloys for large parts such as turbine vanes. It may be possible to use Ir-base alloys for only that part of the airfoil that is exposed to the highest temperatures in turbine vanes. Even more efficient use of the Ir-base alloys may be necessary considering available resources. For example, Ir-base alloys might be used in the higher temperature side in a functionally gradient composite material

Table I. Physical Properties of Pure Ni, Ni-Base Superalloy (MAR-M200), and Pure Ir

	Ideal	Pure Ni	MAR-M200	Pure Ir
Thermal expansion (10^{-6}/°C)	Low	16.3 at 900 °C[29]	15.8 at 982 °C[30]	7.8 at 1000 °C[29]
Thermal conductivity (W/mK)	High	62 at 500 °C[29]		
		88 at RT[29]	24.9 at 982 °C[30]	148 at RT[29]
			8.4 at RT[30]	
Elastic modulus (GPa)	Low	206[30]		524[30]

RT: room temperature.

combined with Ni-base superalloys for the lower temperature side.

V. CONCLUSIONS

We propose a new class of superalloys, termed refractory superalloys, which are defined as alloys with fcc and $L1_2$ coherent structures similar to those of Ni-base superalloys but with considerably higher melting temperatures. Iridium, whose melting point is 2443 °C, was selected as the base metal, and Nb, Ti, Ta, Hf, Zr, and V were added as binary alloying elements. We found that these Ir-base alloys have fcc and $L1_2$ two-phase coherent structures. These refractory superalloys, except for the Ir-V alloy, exhibited very high compressive strengths; 0.2 pct flow stresses at 1800 °C were about 200 MPa, equivalent to those of the strongest W-base refractory alloys. We also found that the strengths of these alloys at 1200 °C were far higher than those of the Ni-base superalloys. In the Ir-base alloys, the three-dimensional maze structure is effective to strengthen the alloy.

ACKNOWLEDGMENTS

We are grateful to Mr. S. Nishikawa, Furuya Metal Co., Ltd., for preparing the Ir-base alloy ingots. We are also grateful to Messrs. N. Sasaki and Y. Matsumoto, Japan Ultra-High Temperature Materials Research Center, for carrying out the compression testing at 1800 °C.

REFERENCES

1. C.T. Sims, N.S. Stoloff, and W.C. Hagel: *Superalloys II*, John Wiley & Sons, New York, NY, 1987, pp. 13 and 551.
2. H. Harada, T. Yamagata, Y. Yokokawa, K. Ohno, and M. Yamazaki: *Proc. 5th Int. Conf. on Creep and Fracture of Engineering Materials and Structures*, B. Wilshire and R.W. Evans, eds., The Institute of Materials, Swansea, United Kingdom, 1993, pp. 255-64.
3. D.B. Miracle and R. Darolia: *Intermetallic Compounds Principles and Practice*, J.H. Westbrook and R.L. Fleischer, eds., John Wiley & Sons, New York, NY, 1995, vol. 2, pp. 53-72.
4. W.F. Brown, Jr., H. Mindin, and C.Y. Ho: *Aerospace Structural Metals Handbook*, CINDAS/Purdue University, Weat Latayette, IN, 1992, vol. 5, pp. 4218 and 5502.
5. T. Yamagata: *Proc. 5th Symp. on High-Performance Materials for Severe Environments*, RIMCOF, Tokyo, Japan, 1994, pp. 107-14.
6. R.L. Fleischer: *Platinum Met. Rev.*, 1992, vol. 36 (3), pp. 138-45.
7. A.M. Gyurko and J.M. Sanchez: *Mater. Sci. Eng.*, 1993, vol. A170, pp. 169-75.
8. Y. Yamabe, Y. Koizumi, H. Murakami, Y. Ro, T. Maruko, and H. Harada: *Scripta Metall. Mater.*, 1996, vol. 35, pp. 211-15.
9. Y. Yamabe-Mitarai, Y. Koizumi, H. Murakami, Y. Ro, T. Maruko, and H. Harada: *Scripta Metall Mater.*, 1997, vol. 36, pp. 393-98.
10. Y. Ro, Y. Koizumi, and H. Harada: *Mater. Sci. Eng.*, 1997, vol. A223, pp. 59-63.
11. *International Tables of Selected Constants 16*, Metals, Thermal and Mechanical Data.
12. *Binary Alloy Phase Diagrams*, T.B. Massalski, ed., ASM INTERNATIONAL, Materials Park, OH, 1992, pp. 2082, 2330, 2355, 2361, and 2366.
13. P. Beardmore, R.G. Davies, and T.L. Johnson: *TMS-AIME*, 1969, vol. 245, pp. 1537-45.
14. G.L. Elickson: *Superalloys 1996*, R.D. Kissinger, D.J. Deye, D.L. Anton, A.D. Cetel, M.V. Nathal, T.M. Pollock, and D.A. Woodford, eds., TMS, Warrendale, PA, 1996, pp. 35-44.
15. D.A. Porter and K.E. Easterling: *Phase Transformations in Metals and Alloys*, Chapman & Hall, London, 1992, pp. 149-60.
16. A.E. Dwight and P.A. Beck: *TMS-AIME*, 1959, vol. 215 pp. 976-79.
17. M.E. Thompson, C.S. Su, and P.W. Voorhees: *Acta Metall. Mater*, 1994, vol. 42 (6), pp. 2107-22.
18. H. Harada, M. Yamazaki, Y. Koizumi, N. Sakuma, N. Fukuya, and H. Kamiya: *Proc. High Temperature Alloys for Gas Turbines*, R. Brunetaund, D. Coutsouradis, T.B. Gibbons, Y. Lindblom, D.B. Meadowcroft, and R. Stickler, eds., D. Reidel Publishing Company, Liege, Belgium, 1982, pp. 721-35.
19. H. Harada, K. Ohno, T. Yamagata, T. Yokokawa, and M. Yamazaki: *Superalloys 1988*, S. Reichman, D.N. Duhl, G. Maurer, S. Antolovich, and C. Lund, eds., TMS, Warrendale, PA, 1988, pp. 733-42.
20. T. Yokokawa, K. Ohno, H. Murakami, T. Kobayashi, T. Yamagata, and H. Harada: *Adv. X-ray Analy.*, 1995, vol. 39, pp. 449-56.
21. D.D. Pearson, F.D. Lemkey, and B.H. Kear: *Superalloys 1980*, J.K. Tien, S.T. Wlodek, H. Morrow III, M. Gell, and G.E. Maurer, eds., ASM, Metals Park, OH, 1980, pp. 513-19.
22. J.K. Tien and R.P. Gamble: *Metall. Trans.*, 1972, vol. 3, pp. 2157-62.
23. P.H. Thornton and R.G. Davies: *Metall. Trans.*, 1970, vol. 1, pp. 549-50.
24. S. Takeuchi and E. Kuramoto: *J. Phys. Soc. Jpn.*, 1971, vol. 31, p. 1282.
25. E.M. Schulman and J.A. Roy: *Acta Metall.*, 1978, vol. 26, pp. 29-37.
26. J.W. Guard and J.H. Westbrook: *TMS-AIME*, 1959, vol. 215, pp. 807-14.
27. D.-M. Wee, O. Noguchi, Y. Oya, and T. Suzuki: *Trans. JIM*, 1980, vol. 21, pp. 237-47.
28. S.M. Brummer, J.L. Birmhall, and C.H. Hengager, Jr.: *Mater. Res. Soc. Symp. Proc.*, D.L. Anton, P.L. Martin, D.B. Miracle, and R. McMeeking, eds., MRS, Pittsburgh, PA, 1990, vol. 194, pp. 257-62.
29. *Metals Reference Book*, 5th ed., C.J. Smithells, ed., Butterworth and Co., London, 1976, p. 942.
30. *ASM Metals Reference Book*, W.H. Cubberly, ed., ASM, Metals Park, OH, 1983.
31. *High Temperature High Strength Nickel Base Alloys*, The International Nickel Company, Inc., 1977, p. 8.
32. D.E. Harasyn, R.L. Heestand, and C.T. Liu: *Mater. Sci. Eng.*, 1994, vol. A187, pp. 138-45.